

Testing a recently proposed scenario for a transplutonian planetoid with the EPM2013 planetary ephemerides

L. Iorio^{1*}

¹*Ministero dell’Istruzione, dell’Università e della Ricerca (M.I.U.R.), Viale Unità di Italia 68 Bari, (BA) 70125, Italy*

26 July 2018

ABSTRACT

By means of the orbital dynamics of the known Sun’s outer planets, we use the just released EPM2013 planetary ephemerides to put on the test the recently proposed hypothesis that one (or more) still unseen super-Earth(s) may lurk at about 200 – 250 astronomical units in the outskirts of the Solar system. Even by conservatively rescaling by a factor of ten the EPM2013 formal uncertainties in the orbital elements of Uranus, Neptune and Pluto over a century (1913–2013), it turns out that their numerically simulated centennial signatures due to a distant perturber 15 times more massive than the Earth located at about 200 astronomical units in an almost circular and ecliptical orbit are far larger, thus making its existence highly unlikely. A careful analysis of the full parameter space of the hypothesized rock-ice planetoid further confirms such a conclusion. Moreover, it turns out that such a body could not exist at less than about 1100 – 1300 astronomical units, thus tightening the previous constraints published in the literature and further justifying the name of Telisto for it.

Key words: Oort Cloud–Kuiper belt: general–gravitation–celestial mechanics–ephemerides

1 INTRODUCTION

New works appeared in the literature (Luhman 2014; Trujillo & Sheppard 2014; Iorio 2014; de la Fuente Marcos & de la Fuente Marcos 2014) have recently renewed the attention on the hypothesis that a still unseen body of planetary size, briefly dubbed as¹ Planet X (PX), may lurk in the remote outskirts of our solar system.

As far as a gaseous giant is concerned, a dedicated direct imaging survey (Luhman 2014) based on an analysis of the data collected by the Wide-field Infrared Survey Explorer (WISE) ruled out the possibility that Saturn-like and Jupiter-like planets can exist at less than 28,000 and 82,000 astronomical units (au), respectively. Moreover, a brown dwarf with a Jovian mass could not exist at less than 24,000 au. Such a study did not deal with smaller rock-ice Earth-sized planetoids, which could well exist at much closer distances.

In this regard, in Trujillo & Sheppard (2014) it was suggested that a still undetected distant super-Earth ($m_X = 2 - 15m_\oplus$) moving in a circular, low inclination orbit between 200 and 300 au could represent a viable explanation for a peculiar pattern concerning the distribution of the arguments of perihelion for some of the known trans-Neptunian objects (TNOs) with perihelion distances $q > 30$ au and semimajor axes $a > 150$ au. Such findings were later sup-

ported in de la Fuente Marcos & de la Fuente Marcos (2014) with a Monte Carlo study of extreme TNOs and comets by even suggesting the possible existence of a pair of trans-Plutonian perturbers² at about 200 and 250 au.

Such claims were criticized in Iorio (2014) on the basis of a brief analysis of the orbital precessions that a hypothetical distant perturber with the physical and orbital characteristics suggested in Trujillo & Sheppard (2014) would necessarily induce on the known planets of the solar system. In fact, the current bounds on the planetary precessions would allow for the existence of such a body at not less than ≈ 500 ($m_X = 2m_\oplus$) – 1000 ($m_X = 15m_\oplus$) au.

Here, we will use the recently released EPM2013 planetary ephemerides (Pitjeva & Pitjev 2014) to independently test the PX scenario proposed in Trujillo & Sheppard (2014); de la Fuente Marcos & de la Fuente Marcos (2014). In particular, we will compare numerically simulated signatures induced by a hypothetical PX on the orbits of Uranus, Neptune and Pluto with the current accuracies in knowing their actual motions as determined in the EPM2013 ephemerides. We will explore the entire parameter space of PX more extensively than ever done so far in the literature by looking at each of its orbital parameter. Finally, we will look at the minimum distance at which PX may exist by inducing orbital perturbations as small as allowed for by the EPM2013 results. Possible objections of lacking of meaningfulness concerning such kind of direct comparisons among theoretically calculated signatures of

* E-mail: lorenzo.iorio@libero.it

¹ Other denominations appeared in the literature so far for such a trans-Neptunian (sometimes defined also as trans-Plutonian) object are Nemesis, Tyche, Telisto.

² Although not explicitly stated, their masses should be of the order of $m_X \approx 10m_\oplus$ (de la Fuente Marcos & de la Fuente Marcos 2014).

a certain dynamical effect and actual data processed without modeling the effect itself have recently proved to be ineffective. Indeed, apart from the fact that such an approach had been proven successful since the time of the Pioneer anomaly (Iorio & Giudice 2006; Standish 2008, 2010; Fienga et al. 2010), the latest constraints on a certain form of the MOND theory, equivalent to the action of a PX located at the same direction of the Galactic Center, which were obtained by explicitly modeling it in a dedicated planetary data reduction (Hees et al. 2014), turned out to be equivalent to those previously established by comparing theoretically computed effects to their observationally inferred counterparts determined without modeling it (Iorio 2010).

2 EXPLORING THE PARAMETER SPACE OF PX

In Table 1, we report the formal uncertainties in the nonsingular orbital elements of the three outer planets of the Solar system resulting from the fitting of the updated models of the EPM2013 ephemerides to an extended data record of more than 800,000 observations ranging from 1913 to 2013 (Pitjeva & Pitjev 2014). In order to make a realistic assessment of their actual accuracy, we will conservatively rescale them by a factor of ten.

In the following, we numerically investigate the orbital perturbations of Uranus, Neptune and Pluto due to a PX with $m_X = 15 m_\oplus$, $a_X = 200$ au, $e_X = 0.01$, $I_X = 10^\circ$ over the same time span of that covered by the observations processed to obtain the EPM2013 ephemerides.

In particular, Figure 1-Figure 6 study the impact of different locations of PX in its orbital plane by varying its true anomaly at the epoch f_0 (Figure 1-Figure 3) and the perihelion ω_X (Figure 4-Figure 6). Figure 7-Figure 9 deal with the orientation of the orbital plane of PX in space: in them, the longitude of the ascending node Ω_X is varied. It turns out that, even by assuming that the realistic orbital uncertainties of the outer planets are ten times larger than those quoted in Table 1, the PX scenario proposed in Trujillo & Sheppard (2014); de la Fuente Marcos & de la Fuente Marcos (2014) is strongly disfavored.

Let us now depart from the main features of the scenario proposed by Trujillo & Sheppard (2014); de la Fuente Marcos & de la Fuente Marcos (2014) by considering more elliptical and inclined orbits of the perturber. In Figure 10-Figure 12, we consider the dependence of the orbital perturbations of Uranus, Neptune and Pluto on the eccentricity of PX. In Figure 13-Figure 15, the orbital signatures induced by a PX moving along inclined orbits are displayed.

Table 1. Formal uncertainties in the nonsingular orbital elements (a : semimajor axis, e : eccentricity, I : inclination, Ω : longitude of the ascending node, ω : argument of perihelion, $\varpi = \Omega + \omega$: longitude of perihelion, M : mean anomaly, $\lambda = \varpi + M$: mean longitude) of the outer planets calculated with the EPM2013 ephemerides. Adapted from Table 10 of Pitjeva & Pitjev (2014). A conservative rescaling factor of the order of ten should be applied to them in order to have realistic uncertainties.

	a (km)	$\sin I \cos \Omega$ (mas)	$\sin I \sin \Omega$ (mas)	$e \cos \varpi$ (mas)	$e \sin \varpi$ (mas)	λ (mas)
Uranus	30.033	3.453	4.007	2.849	2.003	3.592
Neptune	270.479	2.669	5.195	5.546	13.540	12.345
Pluto	2 011.658	2.753	9.931	43.676	31.170	18.088

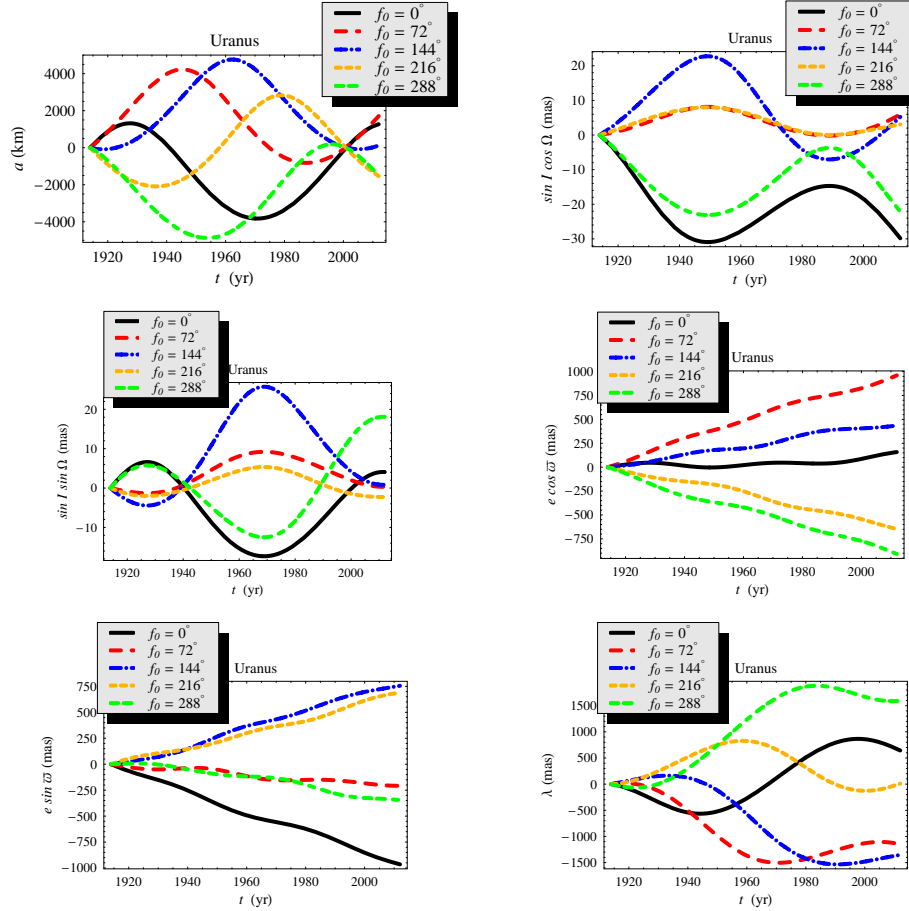


Figure 1. Numerically produced time series of the nonsingular orbital elements a , $\sin I \cos \Omega$, $\sin I \sin \Omega$, $e \cos \varpi$, $e \sin \varpi$, λ of Uranus perturbed by a PX with $m_X = 15 m_\oplus$, $a_X = 200$ au, $e_X = 0.01$, $I_X = 10^\circ$, $\Omega_X = 60^\circ$, $\omega_X = 300^\circ$ for different values of its initial true anomaly f_0 . They were calculated from the differences between two numerical integrations of the equations of motion of Uranus from 1914 to 2012 with and without PX. Both the integrations shared the same initial conditions retrieved from the NASA/JPL database HORIZONS. The amplitudes of the present signals have to be compared with the formal uncertainties (to be conservatively rescaled by a factor of ten) released in Table 10 of Pitjeva & Pitjev (2014).

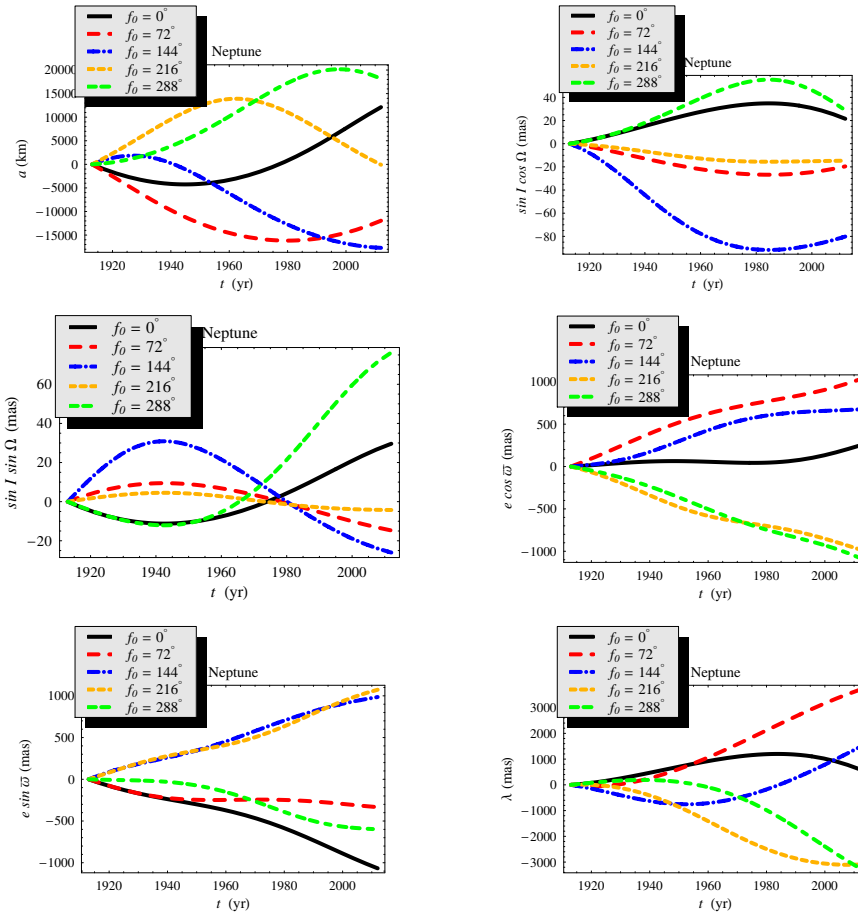


Figure 2. Numerically produced time series of the nonsingular orbital elements a , $\sin I \cos \Omega$, $\sin I \sin \Omega$, $e \cos \varpi$, $e \sin \varpi$, λ of Neptune perturbed by a PX with $m_X = 15 m_\oplus$, $a_X = 200$ au, $e_X = 0.01$, $I_X = 10^\circ$, $\Omega_X = 60^\circ$, $\omega_X = 300^\circ$ for different values of its initial true anomaly f_0 . They were calculated from the differences between two numerical integrations of the equations of motion of Neptune from 1913 to 2012 with and without PX. Both the integrations shared the same initial conditions retrieved from the NASA/JPL database HORIZONS. The amplitudes of the present signals have to be compared with the formal uncertainties (to be conservatively rescaled by a factor of ten) released in Table 10 of Pitjeva & Pitjev (2014).

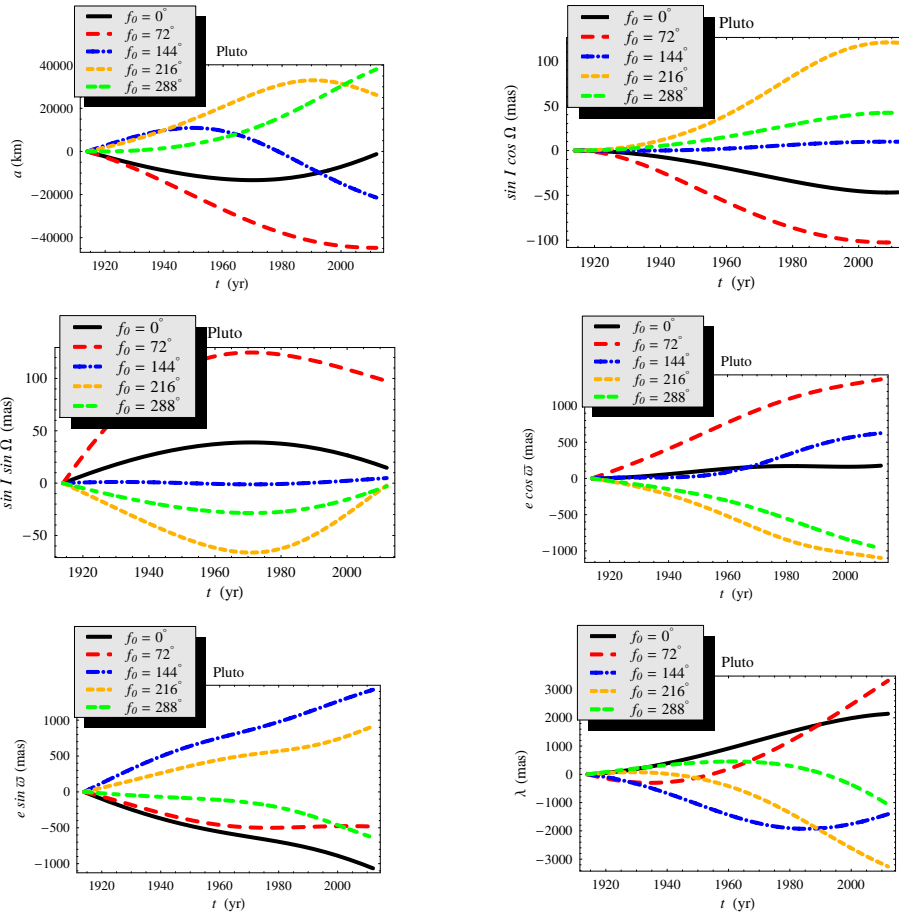


Figure 3. Numerically produced time series of the nonsingular orbital elements a , $\sin I \cos \Omega$, $\sin I \sin \Omega$, $e \cos \varpi$, $e \sin \varpi$, λ of Pluto perturbed by a PX with $m_X = 15 m_\oplus$, $a_X = 200$ au, $e_X = 0.01$, $I_X = 10^\circ$, $\Omega_X = 60^\circ$, $\omega_X = 300^\circ$ for different values of its initial true anomaly f_0 . They were calculated from the differences between two numerical integrations of the equations of motion of Pluto from 1914 to 2012 with and without PX. Both the integrations shared the same initial conditions retrieved from the NASA/JPL database HORIZONS. The amplitudes of the present signals have to be compared with the formal uncertainties (to be conservatively rescaled by a factor of ten) released in Table 10 of Pitjeva & Pitjev (2014).

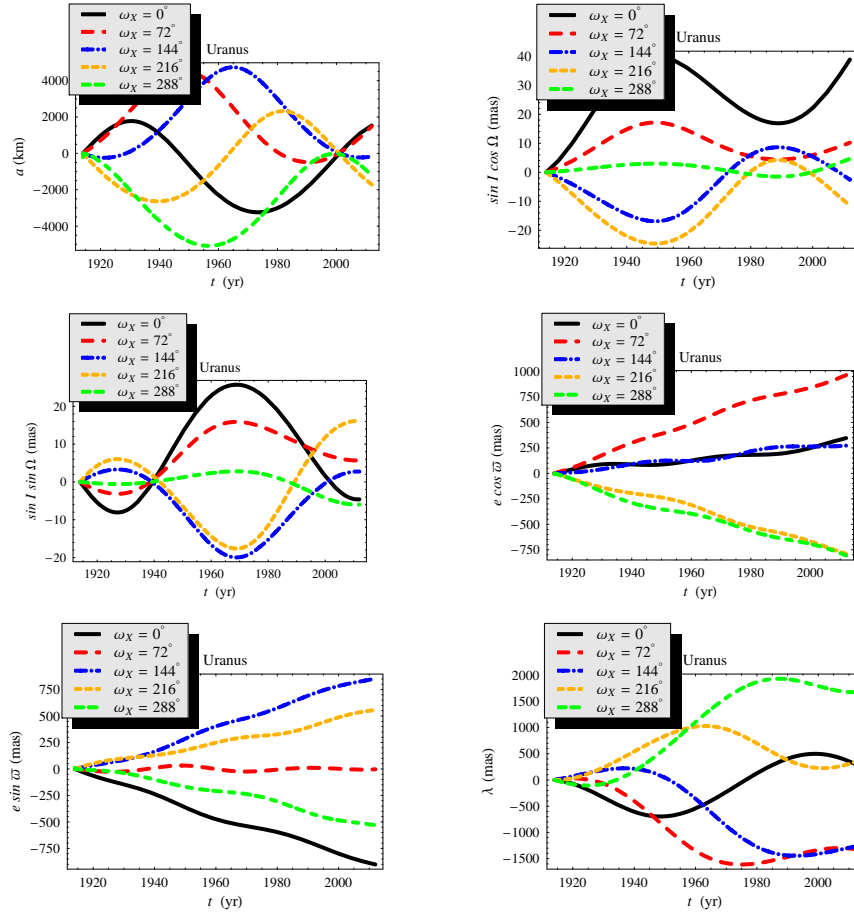


Figure 4. Numerically produced time series of the nonsingular orbital elements a , $\sin I \cos \Omega$, $\sin I \sin \Omega$, $e \cos \varpi$, $e \sin \varpi$, λ of Uranus perturbed by a PX with $m_X = 15 m_\oplus$, $a_X = 200$ au, $e_X = 0.01$, $I_X = 10^\circ$, $f_0 = 72^\circ$, $\Omega_X = 300^\circ$ for different values of its argument of perihelion ω_X . They were calculated from the differences between two numerical integrations of the equations of motion of Uranus from 1914 to 2012 with and without PX. Both the integrations shared the same initial conditions retrieved from the NASA/JPL database HORIZONS. The amplitudes of the present signals have to be compared with the formal uncertainties (to be conservatively rescaled by a factor of ten) released in Table 10 of Pitjeva & Pitjev (2014).

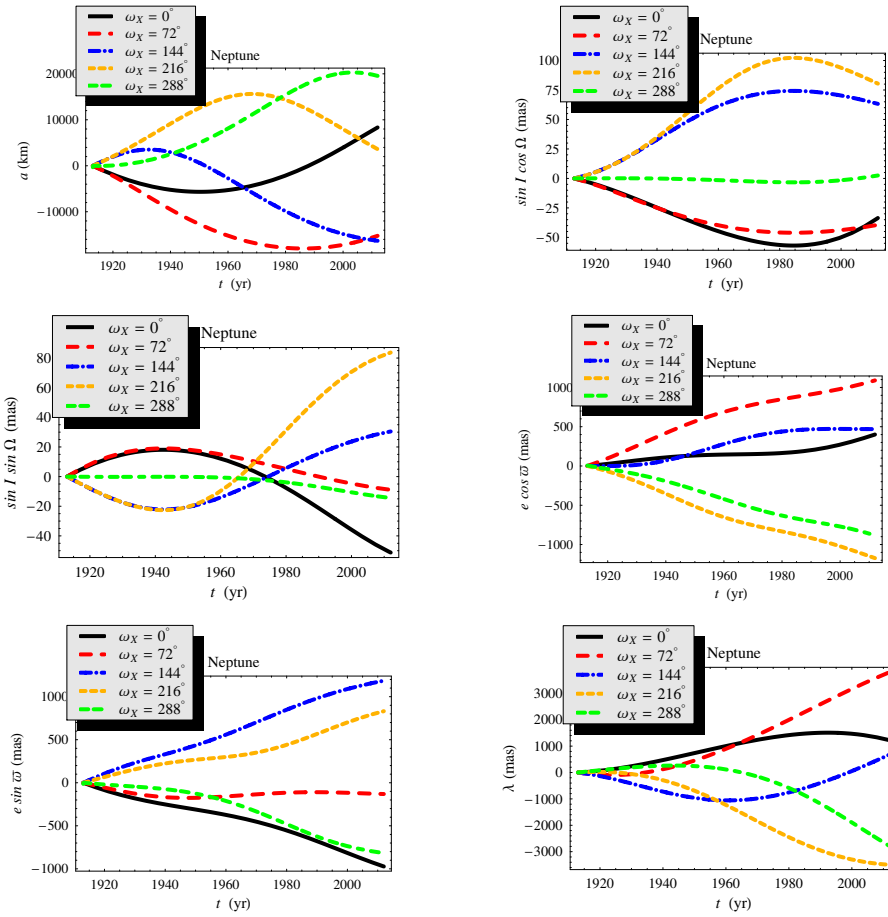


Figure 5. Numerically produced time series of the nonsingular orbital elements a , $\sin I \cos \Omega$, $\sin I \sin \Omega$, $e \cos \varpi$, $e \sin \varpi$, λ of Neptune perturbed by a PX with $m_X = 15 m_\oplus$, $a_X = 200$ au, $e_X = 0.01$, $I_X = 10^\circ$, $\Omega_X = 300^\circ$ for different values of its argument of perihelion ω_X . They were calculated from the differences between two numerical integrations of the equations of motion of Neptune from 1913 to 2012 with and without PX. Both the integrations shared the same initial conditions retrieved from the NASA/JPL database HORIZONS. The amplitudes of the present signals have to be compared with the formal uncertainties (to be conservatively rescaled by a factor of ten) released in Table 10 of Pitjeva & Pitjev (2014).

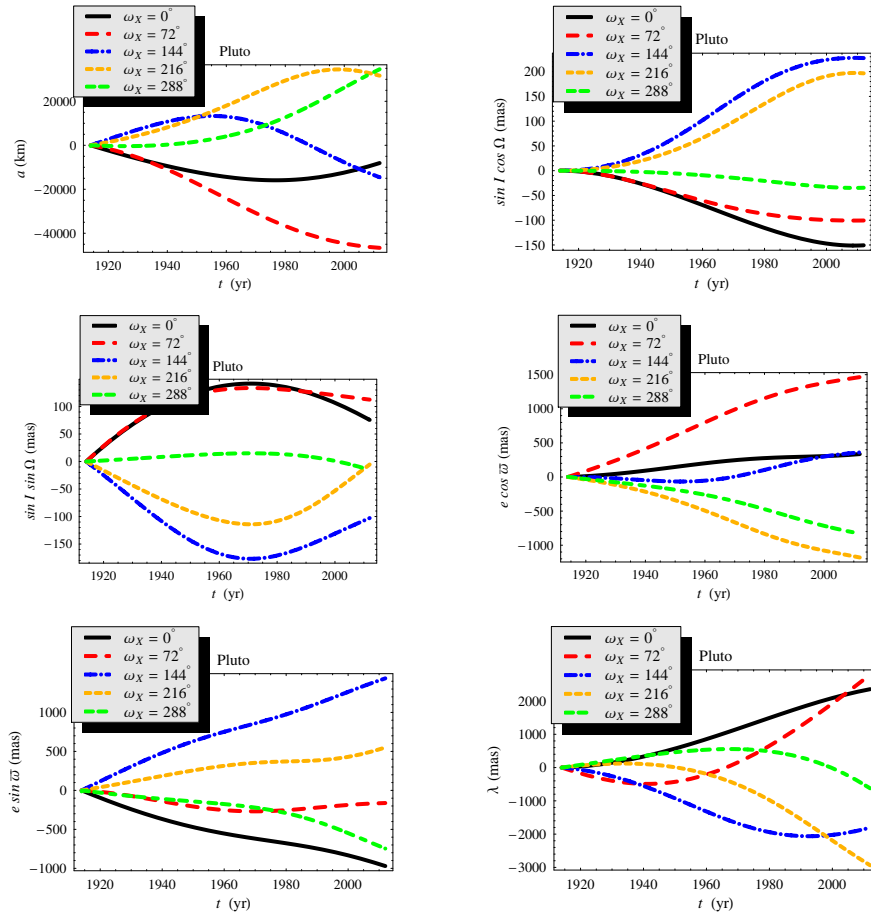


Figure 6. Numerically produced time series of the nonsingular orbital elements a , $\sin I \cos \Omega$, $\sin I \sin \Omega$, $e \cos \varpi$, $e \sin \varpi$, λ of Pluto perturbed by a PX with $m_X = 15 m_\oplus$, $a_X = 200$ au, $e_X = 0.01$, $I_X = 10^\circ$, $f_0 = 72^\circ$, $\Omega_X = 300^\circ$ for different values of its argument of perihelion ω_X . They were calculated from the differences between two numerical integrations of the equations of motion of Pluto from 1914 to 2012 with and without PX. Both the integrations shared the same initial conditions retrieved from the NASA/JPL database HORIZONS. The amplitudes of the present signals have to be compared with the formal uncertainties (to be conservatively rescaled by a factor of ten) released in Table 10 of Pitjeva & Pitjev (2014).

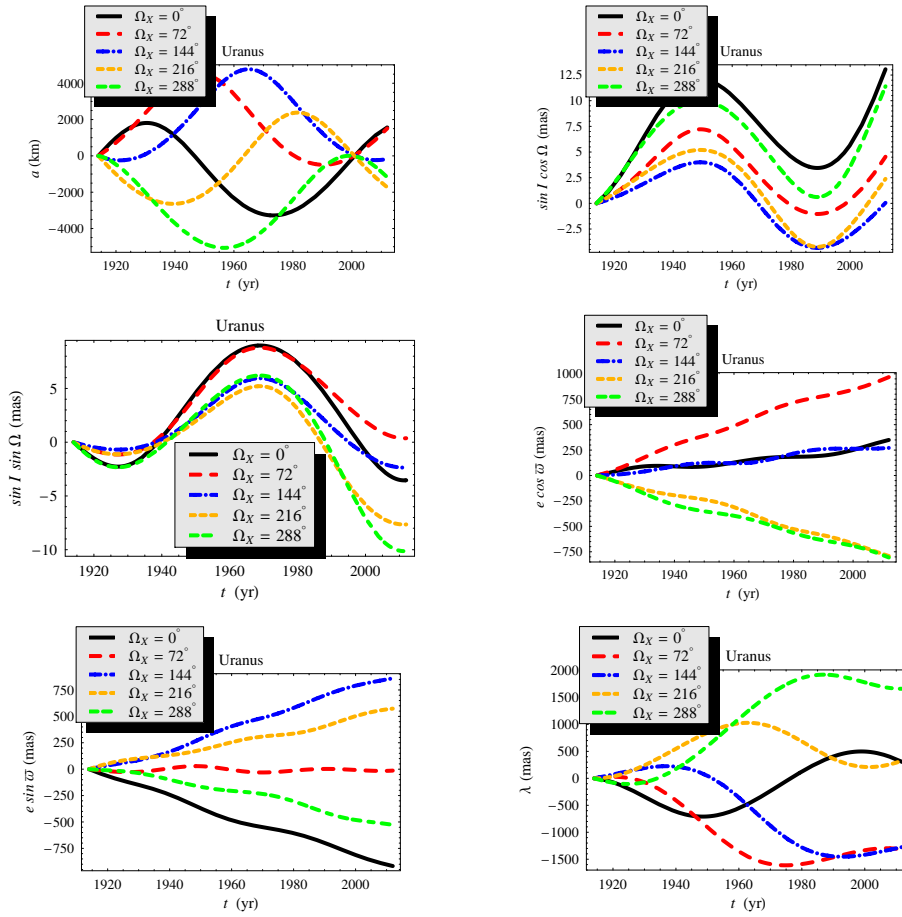


Figure 7. Numerically produced time series of the nonsingular orbital elements a , $\sin I \cos \Omega$, $\sin I \sin \Omega$, $e \cos \varpi$, $e \sin \varpi$, λ of Uranus perturbed by a PX with $m_X = 15 m_\oplus$, $a_X = 200$ au, $e_X = 0.01$, $I_X = 10^\circ$, $f_0 = 72^\circ$, $\omega_X = 300^\circ$ for different values of its longitude of the ascending node Ω_X . They were calculated from the differences between two numerical integrations of the equations of motion of Uranus from 1914 to 2012 with and without PX. Both the integrations shared the same initial conditions retrieved from the NASA/JPL database HORIZONS. The amplitudes of the present signals have to be compared with the formal uncertainties (to be conservatively rescaled by a factor of ten) released in Table 10 of Pitjeva & Pitjev (2014).

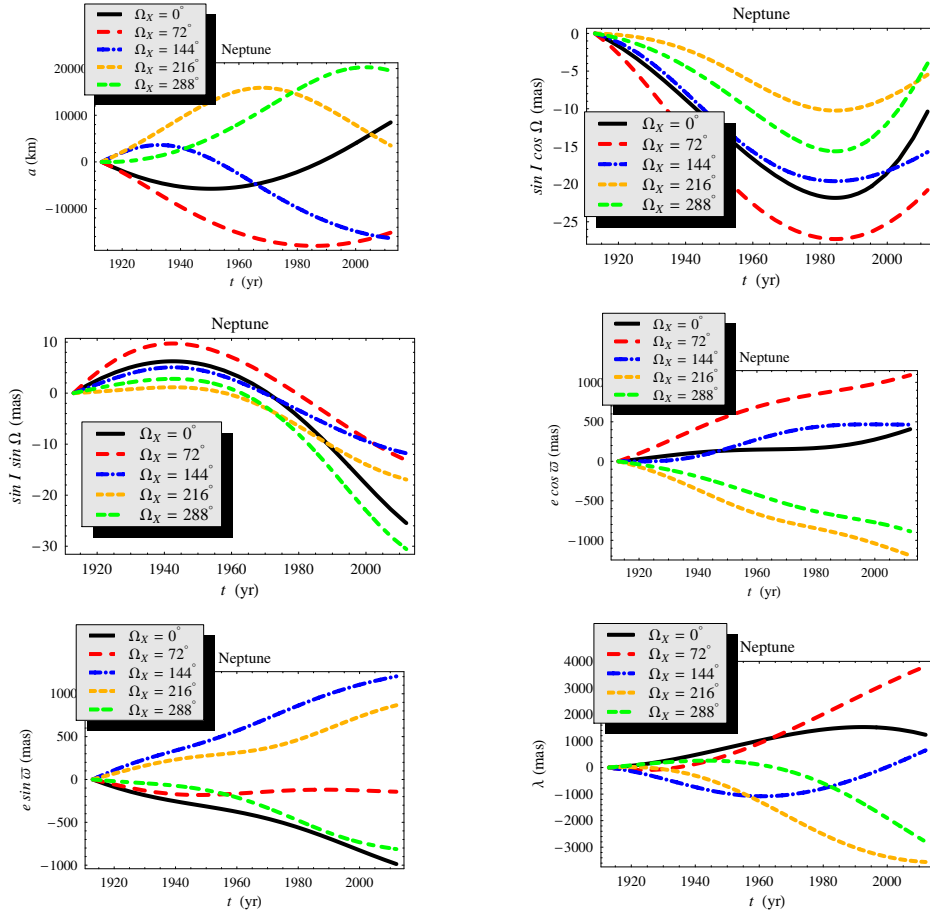


Figure 8. Numerically produced time series of the nonsingular orbital elements a , $\sin I \cos \Omega$, $\sin I \sin \Omega$, $e \cos \varpi$, $e \sin \varpi$, λ of Neptune perturbed by a PX with $m_X = 15 m_\oplus$, $a_X = 200$ au, $e_X = 0.01$, $I_X = 10^\circ$, $f_0 = 72^\circ$, $\omega_X = 300^\circ$ for different values of its longitude of the ascending node Ω_X . They were calculated from the differences between two numerical integrations of the equations of motion of Neptune from 1913 to 2012 with and without PX. Both the integrations shared the same initial conditions retrieved from the NASA/JPL database HORIZONS. The amplitudes of the present signals have to be compared with the formal uncertainties (to be conservatively rescaled by a factor of ten) released in Table 10 of Pitjeva & Pitjev (2014).

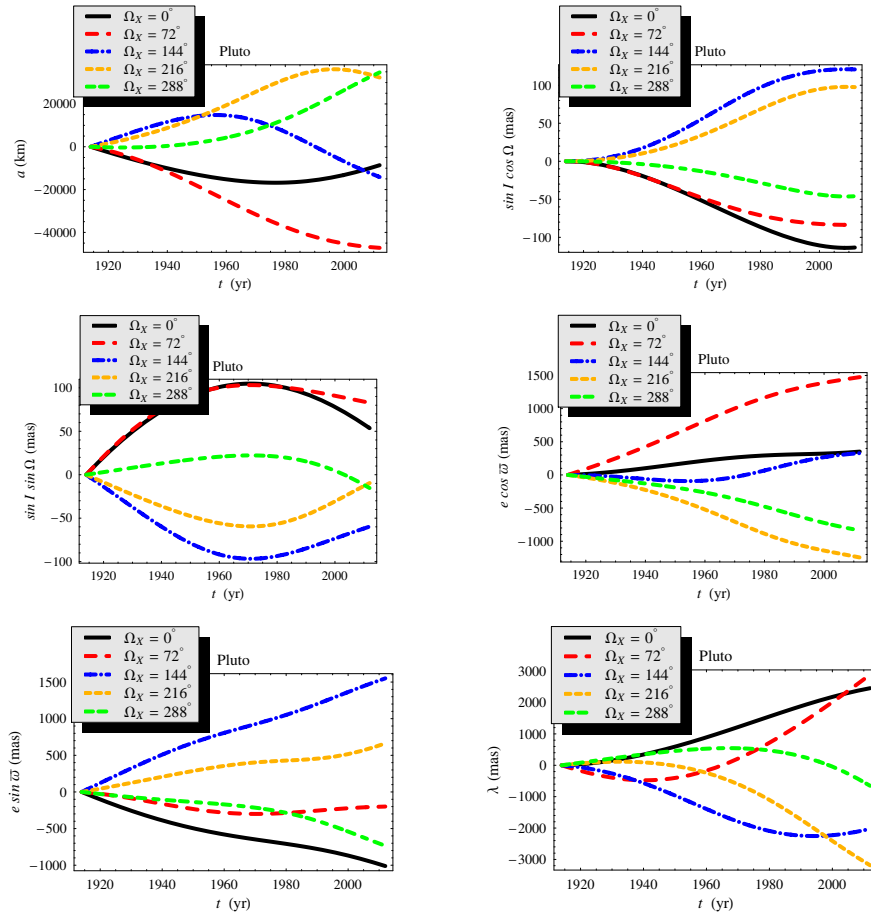


Figure 9. Numerically produced time series of the nonsingular orbital elements a , $\sin I \cos \Omega$, $\sin I \sin \Omega$, $e \cos \varpi$, $e \sin \varpi$, λ of Pluto perturbed by a PX with $m_X = 15 m_\oplus$, $a_X = 200$ au, $e_X = 0.01$, $I_X = 10^\circ$, $f_0 = 72^\circ$, $\omega_X = 300^\circ$ for different values of its longitude of the ascending node Ω_X . They were calculated from the differences between two numerical integrations of the equations of motion of Pluto from 1914 to 2012 with and without PX. Both the integrations shared the same initial conditions retrieved from the NASA/JPL database HORIZONS. The amplitudes of the present signals have to be compared with the formal uncertainties (to be conservatively rescaled by a factor of ten) released in Table 10 of Pitjeva & Pitjev (2014).

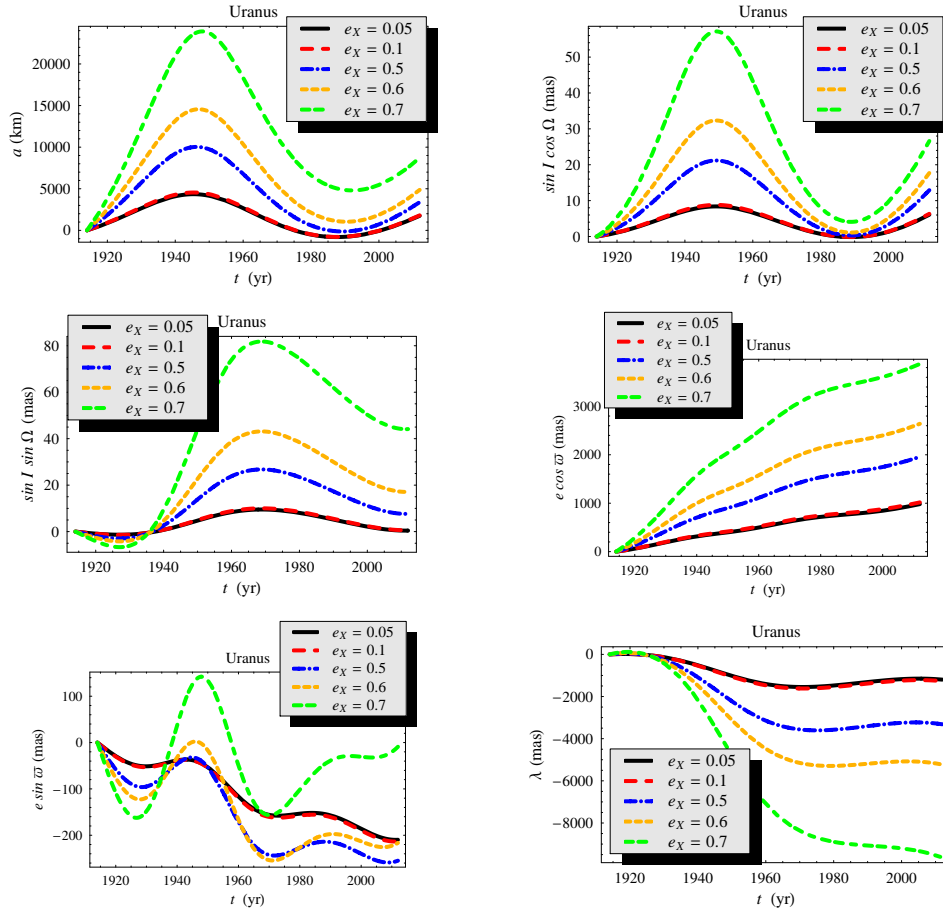


Figure 10. Numerically produced time series of the nonsingular orbital elements a , $\sin I \cos \Omega$, $\sin I \sin \Omega$, $e \cos \varpi$, $e \sin \varpi$, λ of Uranus perturbed by a PX with $m_X = 15 m_\oplus$, $a_X = 200$ au, $I_X = 10^\circ$, $f_0 = 72^\circ$, $\Omega_X = 60^\circ$, $\omega_X = 300^\circ$ for different values of its eccentricity e_X . They were calculated from the differences between two numerical integrations of the equations of motion of Uranus from 1914 to 2012 with and without PX. Both the integrations shared the same initial conditions retrieved from the NASA/JPL database HORIZONS. The amplitudes of the present signals have to be compared with the formal uncertainties (to be conservatively rescaled by a factor of ten) released in Table 10 of Pitjeva & Pitjev (2014).

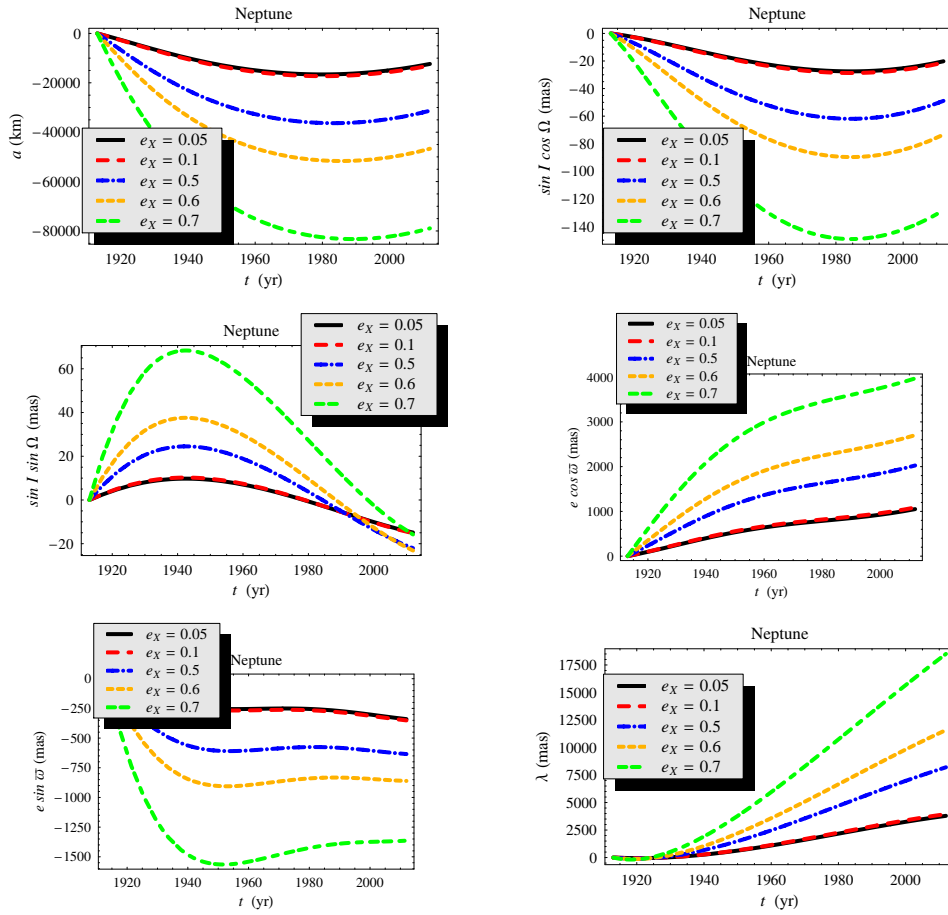


Figure 11. Numerically produced time series of the nonsingular orbital elements a , $\sin I \cos \Omega$, $\sin I \sin \Omega$, $e \cos \varpi$, $e \sin \varpi$, λ of Neptune perturbed by a PX with $m_X = 15 m_\oplus$, $a_X = 200$ au, $I_X = 10^\circ$, $f_0 = 72^\circ$, $\Omega_X = 60^\circ$, $\omega_X = 300^\circ$ for different values of its eccentricity e_X . They were calculated from the differences between two numerical integrations of the equations of motion of Neptune from 1913 to 2012 with and without PX. Both the integrations shared the same initial conditions retrieved from the NASA/JPL database HORIZONS. The amplitudes of the present signals have to be compared with the formal uncertainties (to be conservatively rescaled by a factor of ten) released in Table 10 of Pitjeva & Pitjev (2014).

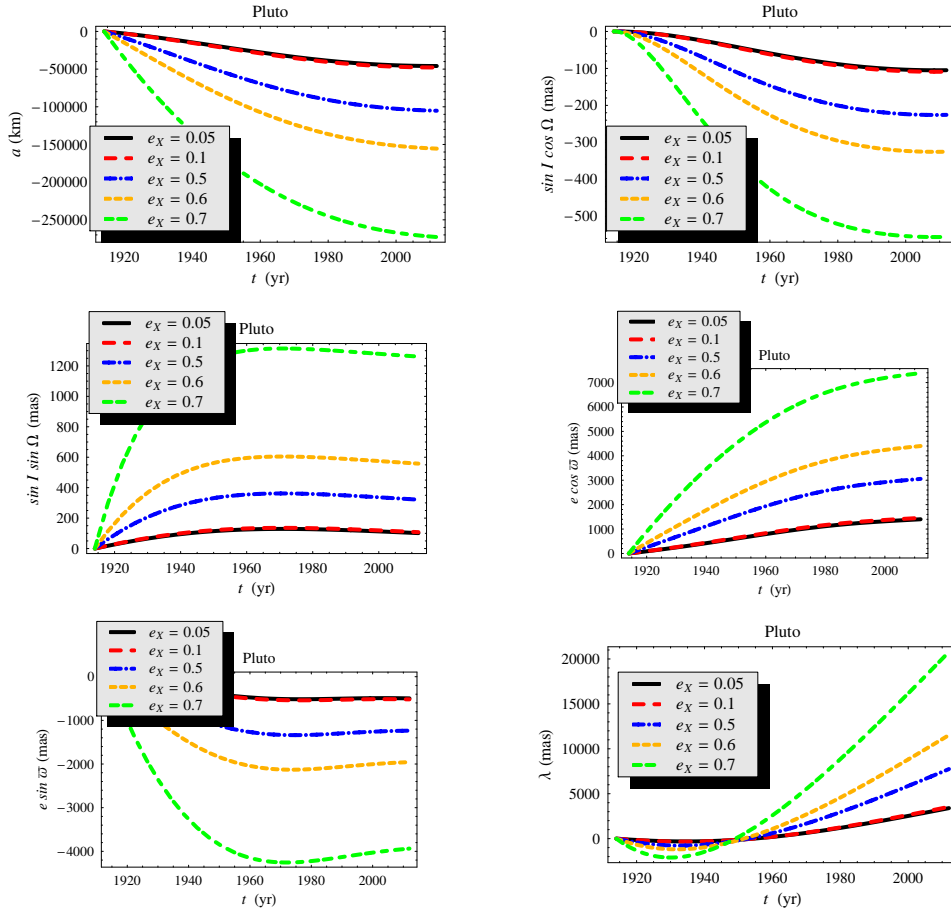


Figure 12. Numerically produced time series of the nonsingular orbital elements a , $\sin I \cos \Omega$, $\sin I \sin \Omega$, $e \cos \varpi$, $e \sin \varpi$, λ of Pluto perturbed by a PX with $m_X = 15 m_\oplus$, $a_X = 200$ au, $I_X = 10^\circ$, $f_0 = 72^\circ$, $\Omega_X = 60^\circ$, $\omega_X = 300^\circ$ for different values of its eccentricity e_X . They were calculated from the differences between two numerical integrations of the equations of motion of Pluto from 1914 to 2012 with and without PX. Both the integrations shared the same initial conditions retrieved from the NASA/JPL database HORIZONS. The amplitudes of the present signals have to be compared with the formal uncertainties (to be conservatively rescaled by a factor of ten) released in Table 10 of Pitjeva & Pitjev (2014).

By allowing for larger distances of PX yields the signatures displayed in Figure 16-Figure 18.

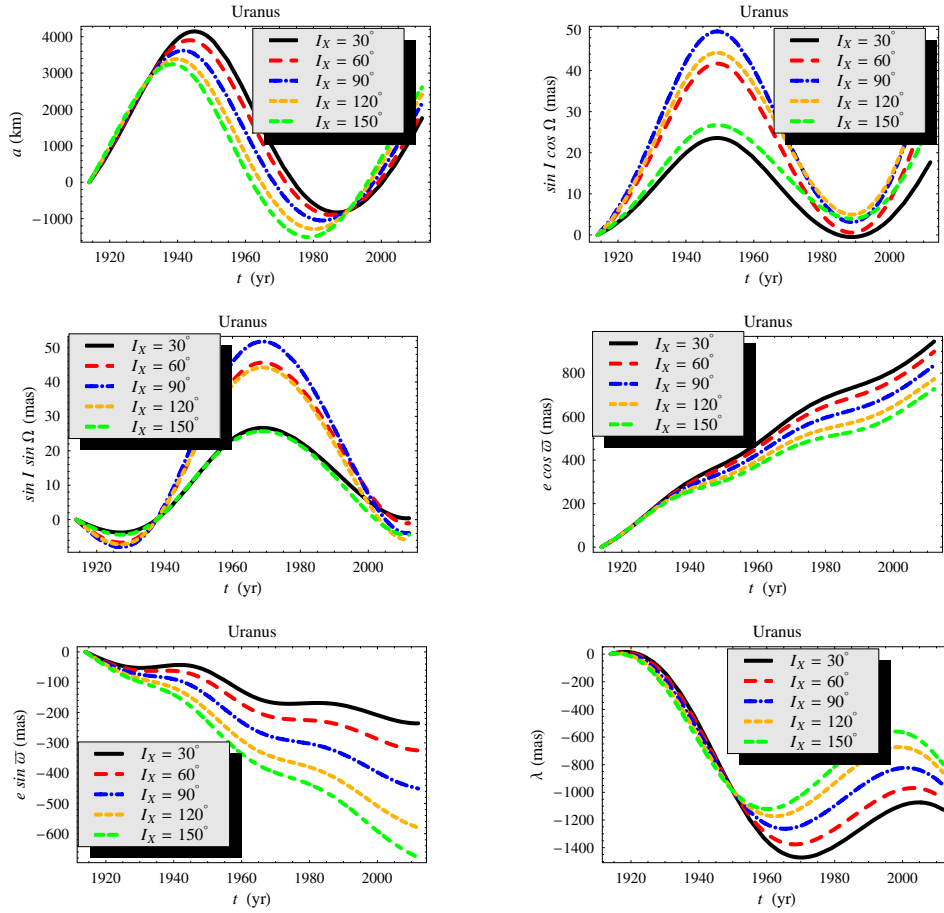


Figure 13. Numerically produced time series of the nonsingular orbital elements a , $\sin I \cos \Omega$, $\sin I \sin \Omega$, $e \cos \varpi$, $e \sin \varpi$, λ of Uranus perturbed by a PX with $m_X = 15 m_\oplus$, $a_X = 200$ au, $e_X = 0.01$, $f_0 = 72^\circ$, $\Omega_X = 60^\circ$, $\omega_X = 300^\circ$ for different values of its inclination I_X . They were calculated from the differences between two numerical integrations of the equations of motion of Uranus from 1914 to 2012 with and without PX. Both the integrations shared the same initial conditions retrieved from the NASA/JPL database HORIZONS. The amplitudes of the present signals have to be compared with the formal uncertainties (to be conservatively rescaled by a factor of ten) released in Table 10 of Pitjeva & Pitjev (2014).

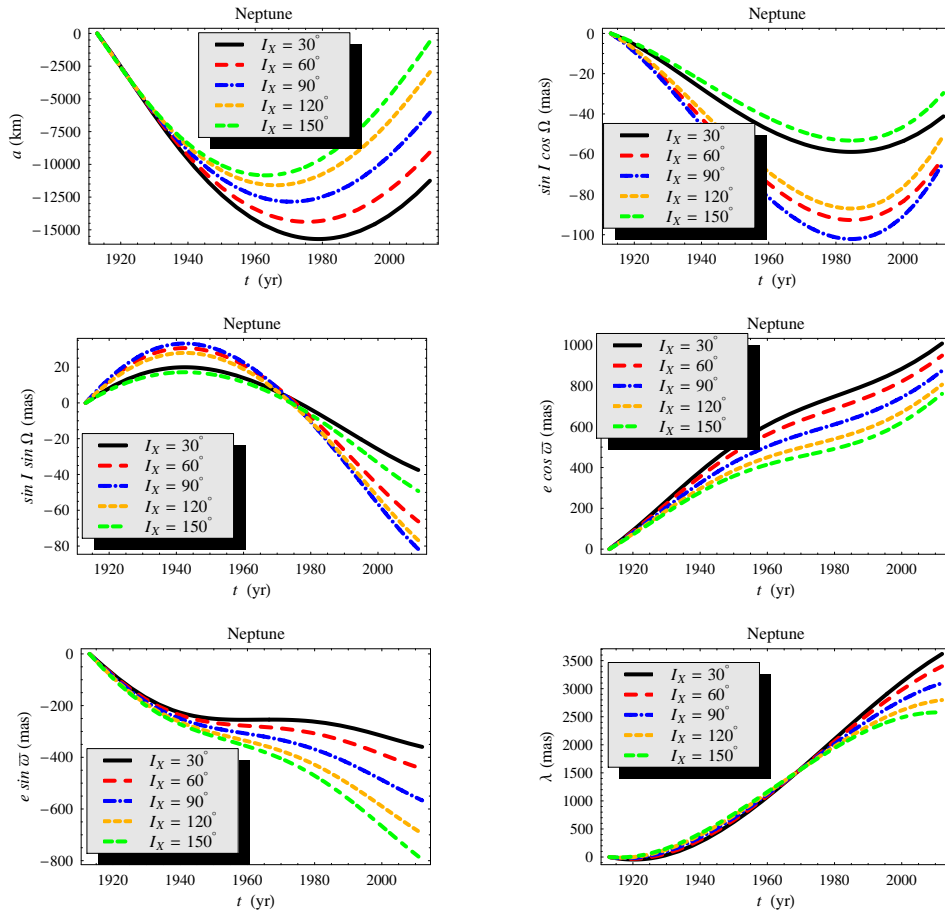


Figure 14. Numerically produced time series of the nonsingular orbital elements a , $\sin I \cos \Omega$, $\sin I \sin \Omega$, $e \cos \varpi$, $e \sin \varpi$, λ of Neptune perturbed by a PX with $m_X = 15 m_\oplus$, $a_X = 200$ au, $e_X = 0.01$, $f_0 = 72^\circ$, $\Omega_X = 60^\circ$, $\omega_X = 300^\circ$ for different values of its inclination I_X . They were calculated from the differences between two numerical integrations of the equations of motion of Neptune from 1913 to 2012 with and without PX. Both the integrations shared the same initial conditions retrieved from the NASA/JPL database HORIZONS. The amplitudes of the present signals have to be compared with the formal uncertainties (to be conservatively rescaled by a factor of ten) released in Table 10 of Pitjeva & Pitjev (2014).

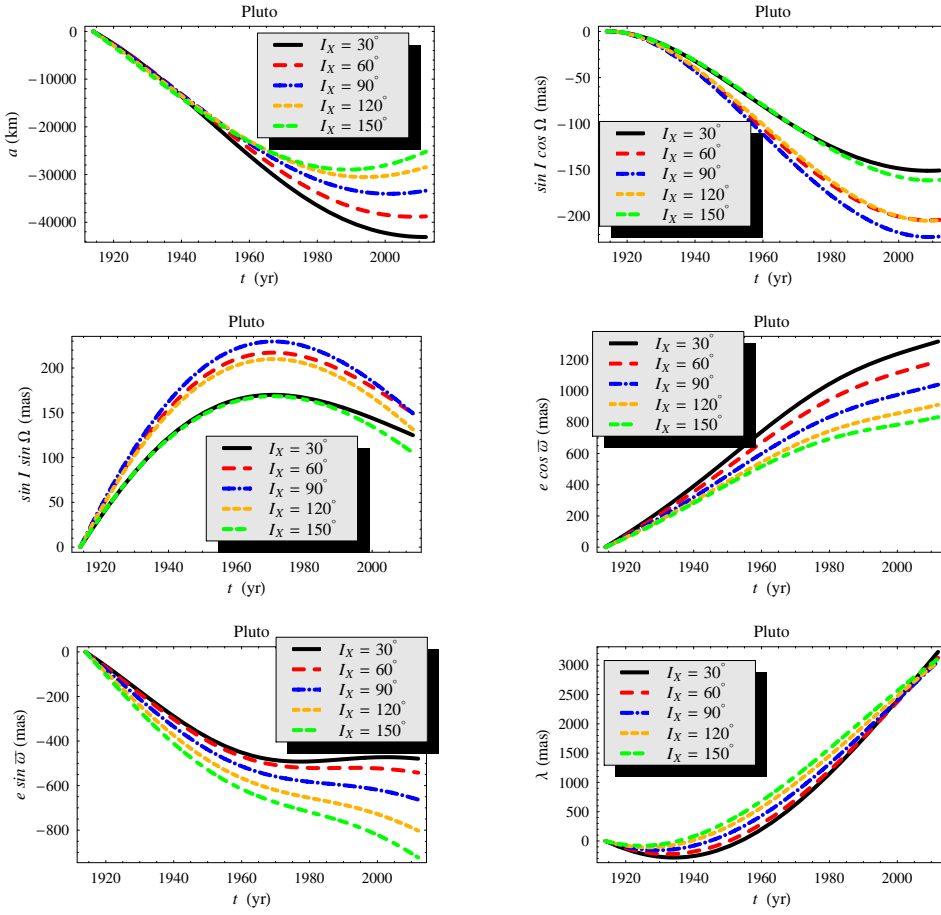


Figure 15. Numerically produced time series of the nonsingular orbital elements a , $\sin I \cos \Omega$, $\sin I \sin \Omega$, $e \cos \varpi$, $e \sin \varpi$, λ of Pluto perturbed by a PX with $m_X = 15 m_\oplus$, $a_X = 200$ au, $e_X = 0.01$, $f_0 = 72^\circ$, $\Omega_X = 60^\circ$, $\omega_X = 300^\circ$ for different values of its inclination I_X . They were calculated from the differences between two numerical integrations of the equations of motion of Pluto from 1914 to 2012 with and without PX. Both the integrations shared the same initial conditions retrieved from the NASA/JPL database HORIZONS. The amplitudes of the present signals have to be compared with the formal uncertainties (to be conservatively rescaled by a factor of ten) released in Table 10 of Pitjeva & Pitjev (2014).

In this case, Uranus and, to a lesser extent, Neptune are the most effective in constraining the minimum distance at which a PX with $m_X = 15 m_\oplus$ can be located. Indeed, the Uranian perturbations of $e \cos \varpi$, $e \sin \varpi$, λ in Figure 16 are larger than the corresponding formal uncertainties of Table 1 by a factor of twenty even for $a_X = 1100 - 1300$ au. In the case of Neptune (Figure 17), the signatures of $e \cos \varpi$ and λ for $a_X = 1300$ au are 4 and 6 times larger than the corresponding formal uncertainties in Table 1, respectively. Figure 18 shows that the Plutonian signature of the mean longitude λ due to a PX at $a_X = 1300$ au is just 1.4 times larger than the formal uncertainty in Table 1.

tive body would induce on the motions of Uranus, Neptune and Pluto are far too large with respect to the formal errors in their orbital elements over a century released by the EPM2013 planetary ephemerides, even if conservatively rescaled by a factor of ten to obtain realistic uncertainties.

Moreover, the latest results from the EPM2013 ephemerides allow us to refine and further tightening the existing constraints on the minimum distance of such a hypothetical distant perturber. Indeed, it turns out that, if really existing, it could not likely be located at less than about 1100 – 1300 au, thus well deserving the name of Telisto recently suggested in the literature.

REFERENCES

- de la Fuente Marcos C., de la Fuente Marcos R., 2014, *Monthly Notices of the Royal Astronomical Society*, 443, L59
- Fienga A., Laskar J., Kuchynka P., Le Poncin-Lafitte C., Manche H., Gastineau M., 2010, in Klioner S. A., Seidelmann P. K., Sof-fel M. H., eds, *IAU Symposium Vol. 261 of IAU Symposium, Gravity tests with INPOP planetary ephemerides*. pp 159–169
- Hees A., Folkner W. M., Jacobson R. A., Park R. S., 2014, *Physical Review D*, 89, 102002
- Iorio L., 2010, *The Open Astronomy Journal*, 3, 1
- Iorio L., 2014, *Monthly Notices of the Royal Astronomical Society*
- Iorio L., Giudice G., 2006, *New Astronomy*, 11, 600
- Luhman K. L., 2014, *The Astrophysical Journal*, 781, 4
- Pitjeva E. V., Pitjev N. P., 2014, *Celestial Mechanics and Dynamical Astronomy*, 119, 237
- Standish E. M., 2008, in Macias A., Lämmerzahl C., Camacho A., eds, *Recent Developments in Gravitation and Cosmology Vol. 977 of American Institute of Physics Conference Series, Planetary and Lunar Ephemerides: testing alternate gravitational theories*. pp 254–263
- Standish E. M., 2010, in Klioner S. A., Seidelmann P. K., Sof-fel M. H., eds, *IAU Symposium Vol. 261 of IAU Symposium, Testing alternate gravitational theories*. pp 179–182
- Trujillo C. A., Sheppard S. S., 2014, *Nature*, 507, 471

3 SUMMARY AND CONCLUSIONS

The possibility that a still undetected rock-ice planetoid about 15 times more massive than the Earth may lurk in the remote peripheries of the Solar system moving at about 200 au along an almost circular and ecliptical trajectory, recently proposed in the literature to explain certain observed features in the distribution of the trans-Neptunian objects populating the Kuiper belt, is strongly disfavoured by the latest advances in the field of the planetary orbit determination. Indeed, the orbital perturbations that such a puta-

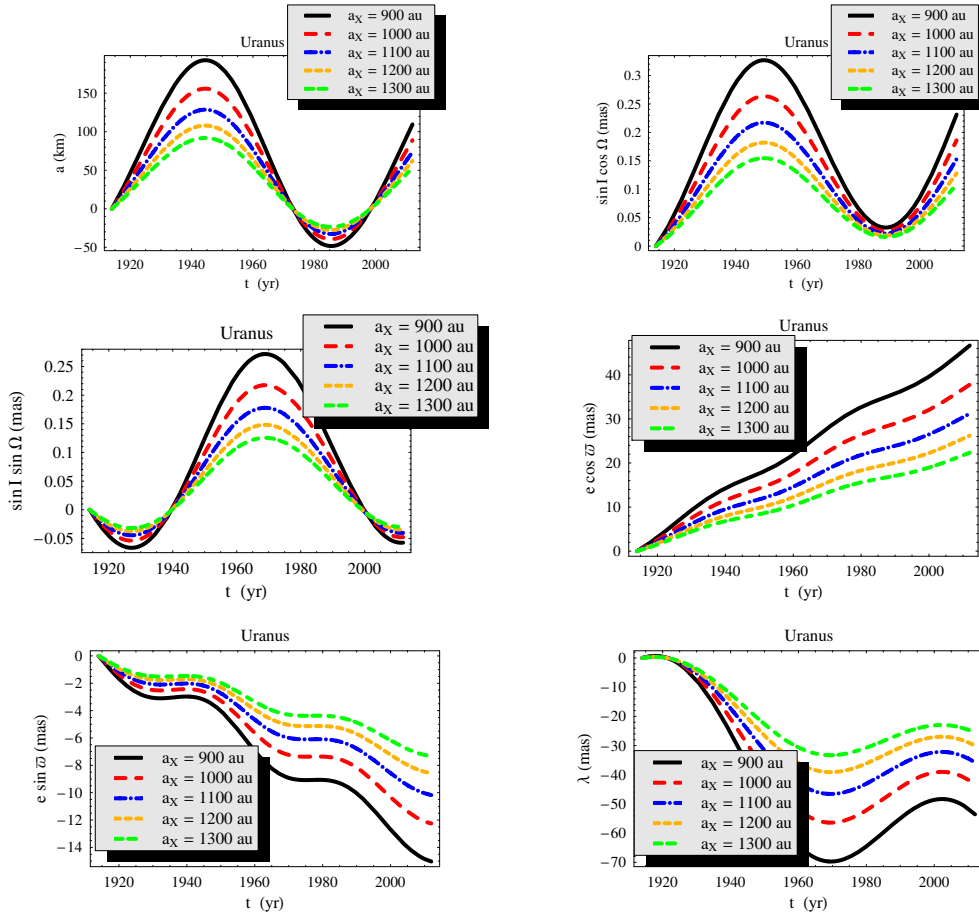


Figure 16. Numerically produced time series of the nonsingular orbital elements a , $\sin I \cos \Omega$, $\sin I \sin \Omega$, $e \cos \varpi$, $e \sin \varpi$, λ of Uranus perturbed by a PX with $m_X = 15 m_\oplus$, $e_X = 0.01$, $I_X = 10^\circ$, $f_0 = 72^\circ$, $\Omega_X = 60^\circ$, $\omega_X = 300^\circ$ for different values of its semimajor axis a_X . They were calculated from the differences between two numerical integrations of the equations of motion of Uranus from 1914 to 2012 with and without PX. Both the integrations shared the same initial conditions retrieved from the NASA/JPL database HORIZONS. The amplitudes of the present signals have to be compared with the formal uncertainties (to be conservatively rescaled by a factor of ten) released in Table 10 of Pitjeva & Pitjev (2014).

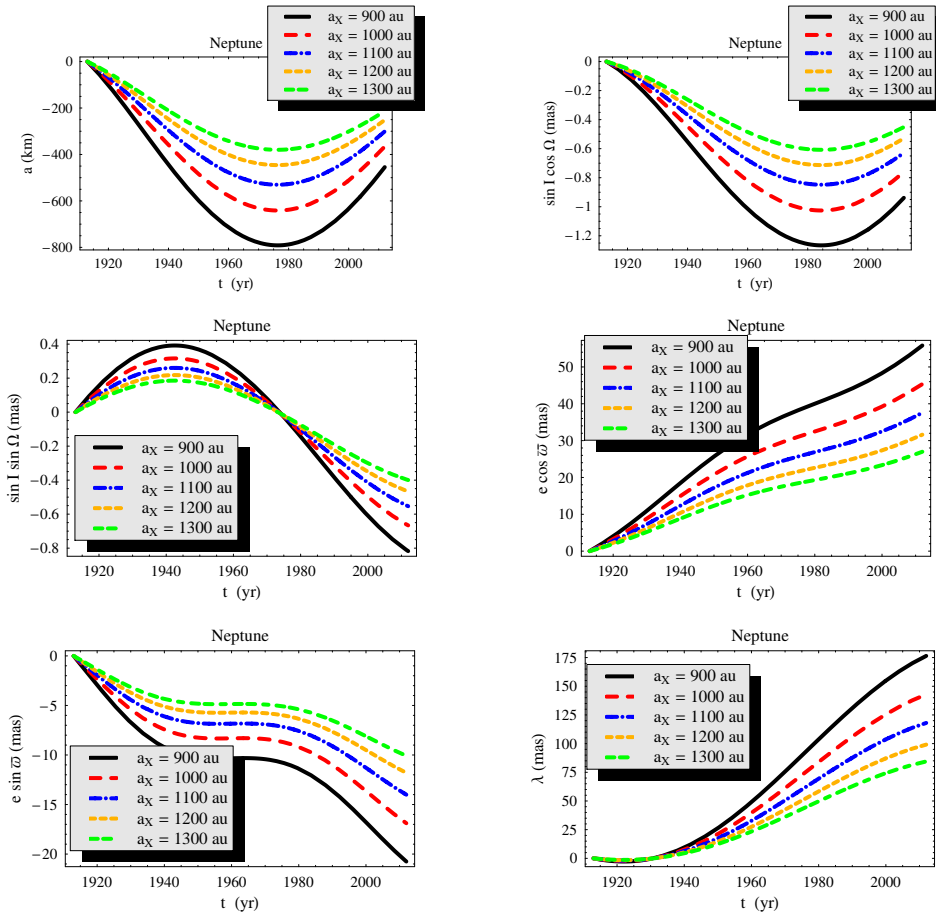


Figure 17. Numerically produced time series of the nonsingular orbital elements a , $\sin I \cos \Omega$, $\sin I \sin \Omega$, $e \cos \varpi$, $e \sin \varpi$, λ of Neptune perturbed by a PX with $m_X = 15 m_\oplus$, $e_X = 0.01$, $I_X = 10^\circ$, $f_0 = 72^\circ$, $\Omega_X = 60^\circ$, $\omega_X = 300^\circ$ for different values of its semimajor axis a_X . They were calculated from the differences between two numerical integrations of the equations of motion of Neptune from 1913 to 2012 with and without PX. Both the integrations shared the same initial conditions retrieved from the NASA/JPL database HORIZONS. The amplitudes of the present signals have to be compared with the formal uncertainties (to be conservatively rescaled by a factor of ten) released in Table 10 of Pitjeva & Pitjev (2014).

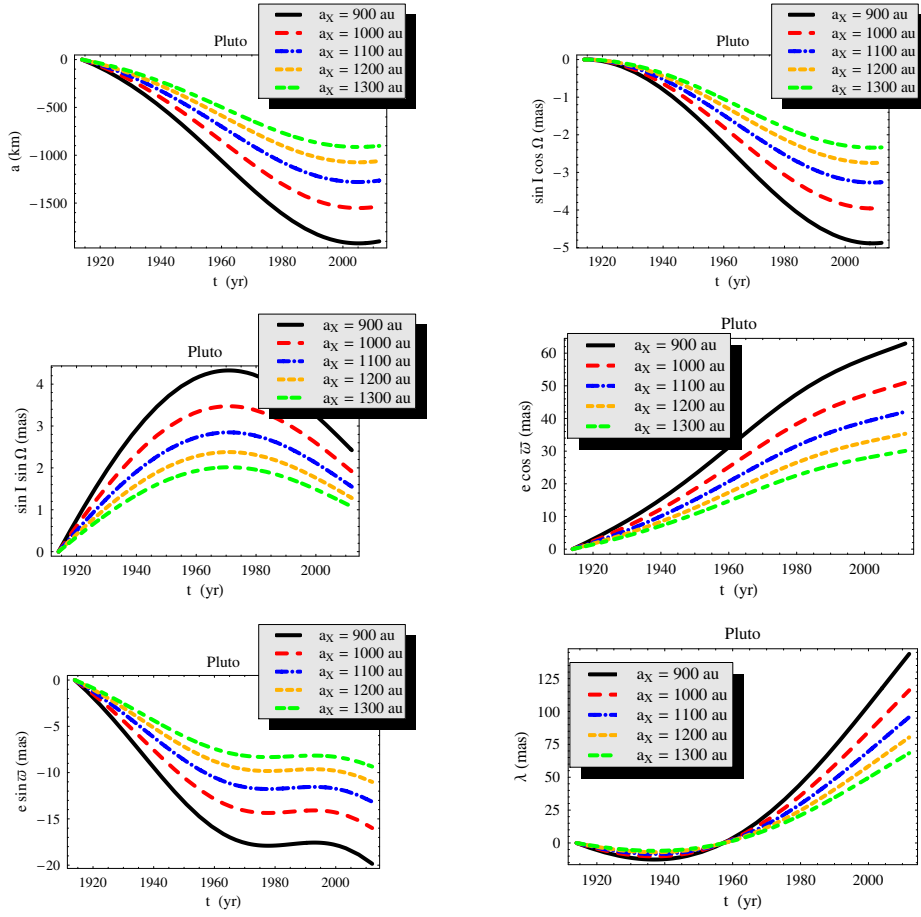


Figure 18. Numerically produced time series of the nonsingular orbital elements a , $\sin I \cos \Omega$, $\sin I \sin \Omega$, $e \cos \varpi$, $e \sin \varpi$, λ of Pluto perturbed by a PX with $m_X = 15 m_\oplus$, $e_X = 0.01$, $I_X = 10^\circ$, $f_0 = 72^\circ$, $\Omega_X = 60^\circ$, $\omega_X = 300^\circ$ for different values of its semimajor axis a_X . They were calculated from the differences between two numerical integrations of the equations of motion of Pluto from 1914 to 2012 with and without PX. Both the integrations shared the same initial conditions retrieved from the NASA/JPL database HORIZONS. The amplitudes of the present signals have to be compared with the formal uncertainties (to be conservatively rescaled by a factor of ten) released in Table 10 of Pitjeva & Pitjev (2014).